Advances in Concrete Construction, *Vol. 8, No. 4* (*2019*) *257-267*
DOI: https://doi.org/10.12989/acc.2019.8.4.257

Numerical analysis of the seismic performance of RHC-PVCT short columns

Jianyang Xue*[1], Xiangbi Zhao[1a], Xiaojun Ke[2], Fengliang Zhang[3] and Linlin Ma[1]

[1]School of Civil Engineering, Xi'an University of Architecture and Technology, Xi'an 710055, China
[2]College of Civil Engineering and Architecture, Guangxi University, Nanning 530004, China
[3]Shaanxi Institute of Architecture Science, Xi'an 710082, China

(*Received December 29, 2018, Revised June 17, 2019, Accepted June 20, 2019*)

Abstract. This paper presents the results of cyclic loading tests on new high-strength concrete (HC) short columns. The seismic performance and deformation capacity of three reinforced high-strength concrete filled Polyvinyl Chloride tube (RHC-PVCT) short columns and one reinforced high-strength concrete (RHC), under pseudo-static tests (PSTs) with vertical axial force was evaluated. The main design parameters of the columns in the tests were the axial compression ratio, confinement type, concrete strength, height-diameter ratio of PVCT. The failure modes, hysteretic curves, skeleton curves of short columns were presented and analyzed. Placing PVCT in the RHC column could be remarkably improved the ultimate strength and energy dissipation of columns. However, no fiber element models have been formulated for computing the seismic responses of RHC-PVCT columns with PVT tubes filled with high-strength concrete. Nonlinear finite element method (FEM) was conducted to predict seismic behaviors. Finite element models were verified through a comparison of FEM results with experimental results. A parametric study was then performed using validated FEM models to investigate the effect of several parameters on the mechanical properties of RHC-PVCT short columns. The parameters study indicated that the concrete strength and the ratio of diameter to height affected the seismic performance of RHC-PVCT short column significantly.

Keywords: high-strength concrete; pseudo-static tests; high-strength concrete filled PVCT; seismic performance; finite element method

1. Introduction

High-strength concrete has the characteristics of high strength, good deformation-resistant, and durability. It could meet the needs of modern engineering structures such as large-span, heavy-load, and high-rise structure development by Ma *et al*. (2016). A series of experiments that the influence on high strength concrete's mode fracture parameters by volume fraction of fiber and maximum aggregate size was conducted by Kumar *et al*. (2017). Murthy *et al*. (2013) concluded the details of development on various high-strength concretes including their mechanical properties.

At the same time, high-strength concrete has some obvious disadvantages, such as low ductility and properties of brittle failure. The common method, improving the deformation capacity of high-strength concrete members, is reducing the spacing of stirrup. However, this method will lead to difficulties in construction and high cost of construction reported by Ma *et al*. (2014). Therefore, more effective and economical methods were urgent found. Based on the related research of composite structures at home and abroad, a new type of confined high-strength concrete column with polyvinyl chloride tubes (PVCT) was proposed.

*Corresponding author, Professor
E-mail: jianyang_xue@163.com
[a]Ph.D. Student

The PVCT was built in the reinforced high-strength concrete column. On the one hand, the concrete protective layer outside the PVCT could isolate the contact between PVCT and the outside world and avoid the aging of PVCT by Breen (2006), Folkman (2014). Because PVCT had better waterproofing performance, it could ensure that core column concrete was not eroded by water by Boersma (2005), Breen (2006). On the other hand, the PVCT restrained the concrete core column and forms a double restraint action with the stirrups. It was beneficial to reduce the number of stirrups, improve the ductility of structural columns, and avoid the collapse of structural columns caused by concrete cracking and shedding under earthquake.

The stress-strain behavior and computational model of the concrete filled composite tube was investigated by Mesbah1a (2017), Borges (2017), Hosseinpour (2015). Kurt (1978), Toutanji *et al*. (2001, 2002) had found through experiments that PVC pipe could reinforced core concrete and improve column ductility, which can be applied in engineering. Based on the test results of a concrete core encased in PVC tubes reinforced with fiber reinforced polymer PVC-FRP by Saafi (2005) equations to predict the ultimate strength and strain of concrete confined with PVC-FRP were developed, and a confinement model for PVC-FRP confined concrete was proposed. Thermoplastic pipe confined concrete (TPCC) overcome the shortcomings of high brittleness of concrete and poor ductility. The strain at peak stress of TPCC was 1.415-5.540 times higher than ordinary concrete, and the energy absorption was 14.8-38.8 times higher than ordinary concrete. The wall thickness and

http://www.techno-press.org/?journal=acc&subpage=7
ISSN: 2287-5301 (Print), 2287-531X (Online)

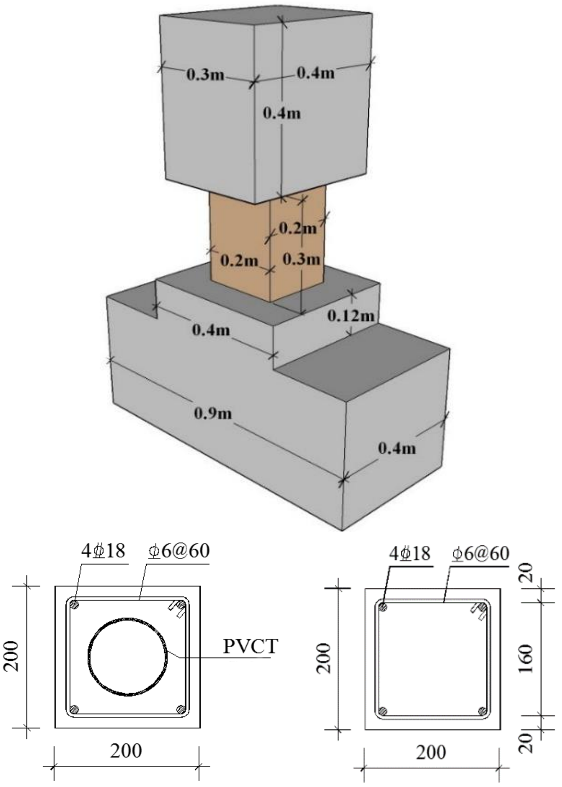

Fig. 1 Geometry of specimens (mm)

(a) RHC-PVCT column (b) RHC column

Fig. 2 Typical reinforcement cages

Table 1 Design parameters of composite columns

Specimens No.	H (mm)	b×h (mm)	f_{cu} (MPa)	λ	n	C_t	t (mm)	L	s
RHC-PVCT-1	300	200×200	75.01	1.5	0.25	PVCT	Φ110×3	4Φ18	Φ6@60
RHC-PVCT-2	300	200×200	79.44	1.5	0.45	PVCT	Φ110×3	4Φ18	Φ6@60
RHC-PVCT-3	300	200×200	75.01	1.5	0.25	PVCT	Φ75×2.3	4Φ18	Φ6@60
RHC	300	200×200	75.01	1.5	0.25	—	—	4Φ18	Φ6@60

Where H denotes the column height, b and h denote the width and height of column cross-section, shear span ratio $\lambda=H/h$, axial compression ratio $n=N/(f_c A_c)$, N denotes the axial compressive load applied to the column, f_c and A_c denote the axial compressive strength of concrete and cross-sectional area of the columns respectively, C_t denotes the confinement type, L denotes the style of longitudinal reinforcement, s denotes the style and spacing of steel bar, t denotes the section size of PVCT.

concrete strength had significant effects on the initial behavior, post-peak behavior and ultimate strength of the stress-strain curve of TPCC by Wang *et al*. (2012). The study by Chen *et al*. (2016) on the numerical investigations were conducted on steel-concrete-PVC double-skin joints under axial compression, in which C3D8R solid element was used to model the PVC tube. The hyperelastic–viscoplastic constitutive model of the rigid PVC proposed via a set of biaxial tests by Ognedal *et al*. (2012) was used to model the PVC inner tube of chord member in the finite element analysis, in which the material properties and stress-strain relations were obtained. They also study is both to investigate the mechanical behavior under various stress triaxialities, induced by different notch radii, and the capabilities of a phenomenological constitutive model by Ognedal *et al*. (2014). Jiang *et al*. (2014) performed testes on the performance of slender concrete-filled CFRP-PVC tubular (CFCT) columns, a nonlinear finite element model (NFEM) was developed to analyze the mechanical properties of long columns by ABAQUS. In these models, 8-node reduced integral format 3D solid elements (C3D8R) were used to model the concrete cores. As well, 4-node reduced integral format shell elements (S4R) were adopted for the PVCT and CFRP.

Mostafa Fakharifar *et al*. (2016) studied the confined concrete-filled polyvinyl-chloride tubular (CCFPT) columns through experimental and analytical studies. Test results indicated that PVC tube provided low confinement on concrete columns but can undergo significant plastic deformation to cope with concrete dilation. PVC tube contributed little to the axial strength of concrete columns by Fakharifar *et al*. (2017). They contrasted the applicability of existing stress-strain models for prediction of CCFPT behavior (2016). Six models by Benzaid *et al*. (2010), Bisby *et al*. (2005), Lam *et al*. (2003), Shehata *et al*. (2002), Wei *et al*. (2012), Youssef *et al*. (2007) were chosen from over 80 models reviewed and reported by Ozbakkaloglu *et al*. (2013).

The research results at home and abroad showed that concrete filled PVCT member can improve the failure characteristics of structural members. Most of the RHC-PVCT members presented plastic failure mode, and improve the bearing capacity, anti-seismic deformation capacity and durability of the structural members. It also had the advantages of low-cost, energy-saving and environmental protection of construction. However, there was no research on reinforced high-strength concrete filled PVCT member. Based on four columns under the PSTs were tested in Xi'an University of Architecture and Technology, this paper studied the seismic performance and deformation capacity of RHC-PVCT column by finite element analysis.

2. Experimental program

2.1 The specimens design

Table 2 Concrete mixture proportions and properties

Materials	f_{cu} (MPa)	E_c (MPa)	Cement (kg/m^3)	Water (kg/m^3)	Fine aggregate (kg/m^3)	Coarse aggregate (kg/m^3)	Fly ash (kg/m^3)	Water reducer (kg/m^3)
High-strength concrete	75.01	40518	482	160	664	1097	121	12
	79.44	41173	533	160	745	1117	121	12

Table 3 Mechanical properties of steel

Materials	Diameter (mm)	Yield strength (MPa)	Tensile strength (MPa)	Modulus of elasticity (MPa)
Steel	Φ6	340	380	1.977×10^5
	Φ18	465	644	2.188×10^5

Table 4 Mechanical properties of PVCT

Materials	Thickness (mm)	Tensile strength (MPa)	Hoop strength (MPa)	Modulus of elasticity (MPa)
PVCT	2.3	19.56	39.12	3075
	3	20.20	40.40	3315

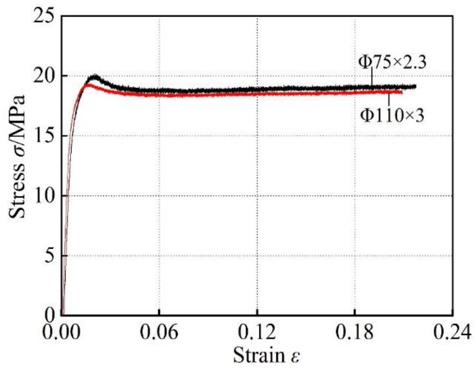

Fig. 3 PVCT specimen stress-strain curve

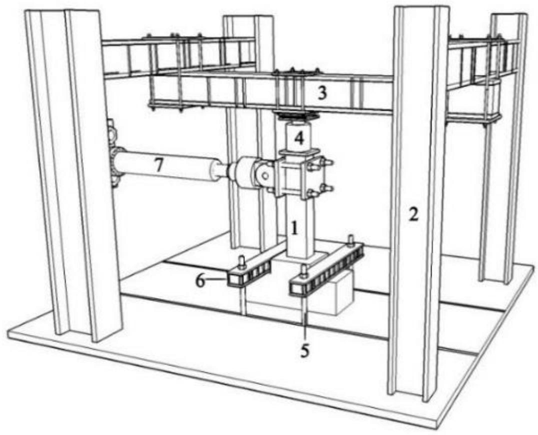

Fig. 4 Test frame, 1-Specimen, 2-Reaction rack, 3-Reaction beam, 4-Hydraulic jack, 5-Anchor bolt, 6-Fixed beam, 7-MTS actuator

The seismic performance of four specimens, including three RHC-PVCT columns and one RHC column, were obtained through PSTs. The influence of diameter of PVCT and axial compression ratio on the mechanical behavior of high-strength concrete filled PVCT column was considered. The design parameters are listed in Table 1. The geometrical dimensions and confinement type of the test piece are shown in Fig. 1 and Figs. 2(a)-(b).

2.2 Material properties

According to the design, the stirrups and longitudinal reinforcement were bound together to form a steel skeleton, and then combined with the PVCT to form whole skeleton.

2.2.1 Concrete

High-strength concrete is agitated with a forced mixer for excellent property. The concrete mixture proportions and properties, including the cube strength (f_{cu}) and modulus of elasticity (E_c), are listed in Table 2.

2.2.2 Steel

According to the Chinese Code for Metallic Materials-Tensile Testing-Method of Test at Ambient Temperature (GB/T228-2002) (2002), all of steel were tested result as listed in Table 3.

2.2.3 PVCT

Follows the Chinese Code for Thermoplastic Pipes-Determination of Tensile Properties-Part 1: General Test Method (GB/T 8804.1-2003) (2003), the strength of the PVCT was measured the uniaxial tensile test (Fig. 3), from which the PVCT tensile strength and elastic modulus can be obtained and illustrated in Table 4. Test stress-strain curves of PVCT samples is shown in Fig. 3.

2.3 Test setup and procedure

The test setup is schematically shown in Fig. 4. The experiment method was used mixed control of load and displacement according to Chinese Code for Specification for the seismic test of buildings (JGJ101-2015) (2015).

The horizontal load of the top of the column was automatically controlled by 500kN Fieldbus Control System (FCS) coordinated loading control system, and the vertical load of the top of the column was imposed by the 2000 KN hydraulic jack. The displacement value of the top of the column was taken as the horizontal displacement at the loading point under various loads. The displacement value was automatically collected by the built-in displacement sensor of the FCS.

All the specimens were subjected to axial compression force under cyclic lateral loads. In the load-controlled stage of this test, the increment of lateral cycle load was 20 kN until the columns yielded. Subsequently, the loading procedure of short columns was changed into the displacement-controlled load. Each displacement loading step was repeated three times until the column failure or lateral load of the column dropped below the 85% ultimate value. During the proposed cyclic loading tests, the loading and unloading rates were similar.

3. Results and discussion

3.1 Hysteresis loops

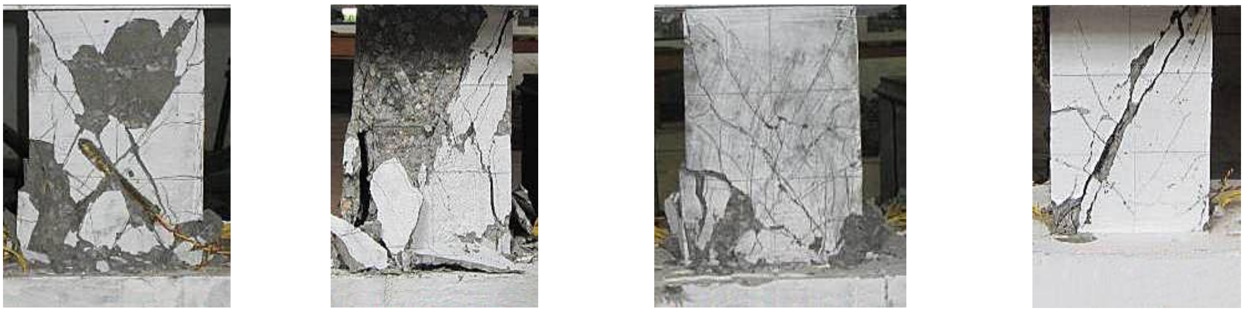

(a) RHC-PVCT-1 (b) RHC-PVCT-2 (c) RHC-PVCT-3 (d) RHC

Fig. 5 Failure modes of specimens

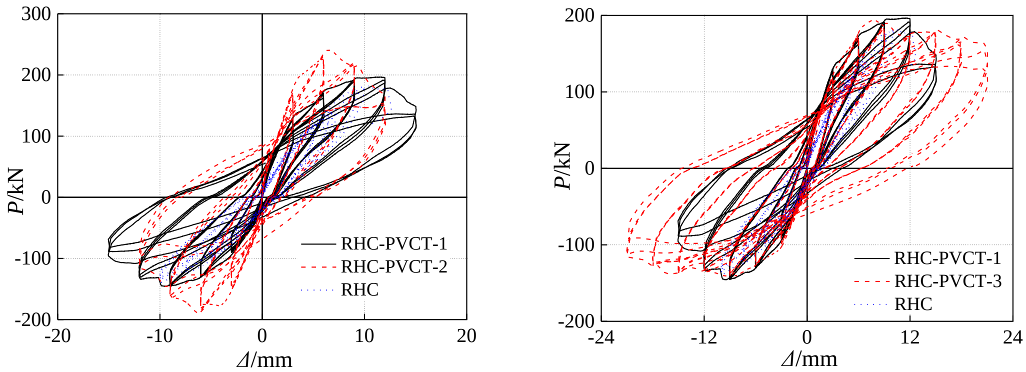

(a) RHC-PVCT-1 column (b) RHC-PVCT-2 column

Fig. 6 Hysteresis loops of short columns

Fig. 5 shows the RHC-PVCT columns appearance X-shaped cross diagonal cracks, because of the core concrete confined by PVCT. In this way, it ensures that more bending and diagonal cracks were formed to dissipate seismic energy in RHC-PVCT columns (Figs. 5 (a)-(d)), and effectively avoid the phenomenon that the forming the main cracks quickly in RHC column (Fig. 5(d)).

Fig. 6 shows the hysteresis curves of the relationships of lateral force and drift ratio for all specimens, where P, Δ and θ are the horizontal load, horizontal displacement and lateral drift ratio at the tops of the columns, respectively.

In the elastic stage of specimens, the hysteretic loops surround area was very small and narrow, and the load-displacement have linear shape. The hysteresis curves of all specimens were stable and not significantly pinched. When loading and unloading within a small drift, the hysteresis loops was almost linearly. In the elasto-plastic stage, the hysteretic curve inclined to the X-axis, the stiffness gradually degenerates. When the cracks began to appear on surface of RHC-PVCT column, the stiffness shown obvious degradation and residual deformation was observed in unloading. The hysteresis curves for the two same-displacement cycles preceding the peak load were nearly identical. In the displacement-controlled stage, with the increased of horizontal displacement, the horizontal bearing capacity continues to improve. In the failure stage, the strength degradation of the RHC-PVCT columns in the second cycle became obviously. With the increase of displacement, the hysteretic curves of the specimens gradually showed obvious difference because of the change of strengthening measures.

As can be seen from Figs. 6(a)-(b), the hysteretic curves of short columns had the following characteristics:

(1) The hysteretic curves with confined area by RHC-PVCT column was fuller than by RHC column, because of the core column in PVCT of RHC-PVCT column can effectively enhance the energy dissipation capacity and deformation ability.

(2) Compared with RHC-PVCT-1 column, the hysteretic curve of RHC-PVCT-3 column was fuller. The energy dissipation of the specimens was obviously affected by the diameter of PVCT. It was also very important to adopt a reasonable area ratio of concrete core column of PVCT.

(3) The area of hysteretic curve of RHC-PVCT-2 column was larger than that of RHC-PVCT-1 column under the condition of similar strength concrete. This indicated that different axial compression ratio had different influences on the hysteresis loops of short columns.

3.2 Skeleton curves

A skeleton curve reflected the relationship between the peak loads and corresponding displacements from the hysteresis loops of the specimens. The skeleton curves of four short columns are sketched in Fig. 7. The loading process was divided into the stage of elastic, elasto-plastic and failure. The ultimate loading for the positive direction was slightly larger than the negative direction.

As shown in Fig. 7, the following features exist:

(1) In the failure stage, the bearing capacity of the RHC column was unstable, the strength decreases rapidly. However, for the RHC-PVCT column, the failure stage of

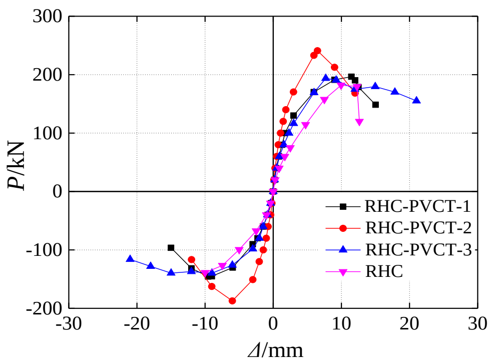

Fig. 7 Comparison of skeleton curves for specimens

skeleton curve was stable, and the ductility was improved. In particular, RHC-PVCT-1 column had increased by 8% for peak load compared to RHC column.

(2) Comparing the skeleton curves of RHC-PVCT-1 column and RHC-PVCT-3 column, it can be seen that as the tube diameter increased, the initial stiffness of the specimen increased, and the peak load increased by about 1.5%. However, RHC-PVCT-1 column in the failure stage, the strength was reduced faster, the stiffness degraded significantly, and the deformation ability was reduced. On the one hand, because the adhesion between the PVCT and the concrete was small bring about easy to slip. On the other hand, when the cross-sectional area remains unchanged, the thickness of concrete protective layer was reduced by increasing the diameter of PVCT, which increasing the difference of deformation ability between the two parts of concrete inside and outside the PVCT. These two reasons jointly led to the earlier cracking for RHC-PVCT-1 column with thin concrete protective layer than RHC-PVCT-3 column. RHC-PVCT-1 column had higher initial stiffness because of its larger diameter and larger area of confined core concrete than RHC-PVCT-3 column. When the load exceeding the peak load, the transverse deformation of core concrete increased sharply, which results in the expansion of PVCT. After the expansion of the interior, the outer concrete protective layer was squeezed, which results in the collapse of concrete at the middle column. It was consistent with the failure phenomena as shown in Fig. 5.

(3) When the concrete strength consistent, the peak load of RHC-PVCT-2 column was 22.6% higher than that of PVC-RHC-1 column. It indicated that the stiffness and strength of the RHC-PVCT column with lower axial pressure were reduced faster, the ultimate deformation smaller, and the ductility was poorer.

4. Numerical analysis using FEM

The finite element software ABAQUS/ Standard 6.12 was used to establish the FEM of the RHC-PVCT column.

4.1 Material model

4.1.1 Material model for the HC

Concrete Damaged Plasticity Model which can well simulate the nonlinear characteristics of concrete was selected. The cross-sections of all columns in this experiment were divided, as shown in Figs. 8(a)-(b).

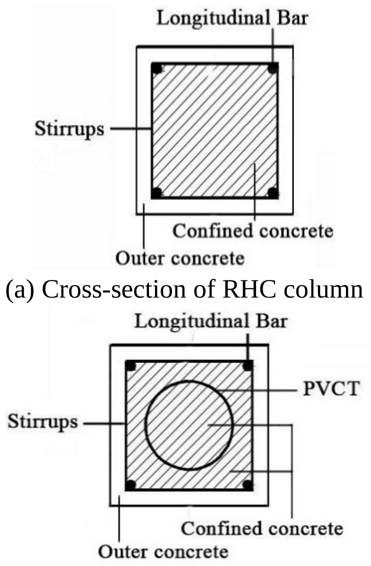

(a) Cross-section of RHC column

(b) Cross-section of RHC-PVCT column

Fig. 8 Material calculation model for the columns

$$y=\begin{cases}\alpha_a x+(3-2\alpha_a)x^2+(\alpha_a-2)x^3 & 0\le x<1\\ \dfrac{x}{\alpha_d(x-1)^2+x} & x\ge 1\end{cases} \tag{1}$$

Where $y=\sigma/f_c$, f_c is peak stress, $x=\varepsilon/\varepsilon_{c0}$, ε_{c0} is the peak strain, α_a, α_d are control parameters of ascending stage and descending stage of curve, respectively.

The fitting results are shown by the Eq. (1) as shown by the red heavy line in Fig. 9.

Fig. 9 shows that when the control parameter α_a of the rising section changes from 0.6 to 1.5 with the increase of HC strength, the fitting curve of the rising section agrees well with the experimental curve. In the downing section, the brittleness of HC was more obvious with the increasing of strength, and the experimental results were discrete large. It was suggested that the range of control parameter in downing section should be between 4 and 15, the higher strength of HC, and the value of α_d was larger.

For the confined concrete in RHC-PVCT column was based on the constitutive relation model by Kent-Park (1982), as shown in Fig. 10.

In the modified Kent and Park relation, the stress-strain relation is

$$f_c=\begin{cases}f_{cc}[\dfrac{2\varepsilon_c}{\varepsilon_{cc}}-(\dfrac{\varepsilon_c}{\varepsilon_{cc}})^2] & 0\le\varepsilon_c<\varepsilon_{cc}\\ f_{cc}[1-Z(\varepsilon_c-\varepsilon_{cc})] & \varepsilon_c\ge\varepsilon_{cc}\end{cases} \tag{2}$$

$$f_{cc}=kf_{c0}^{'} \qquad \varepsilon_{cc}=k\varepsilon_{c0}^{'}$$

Where

$$k=1+\frac{\rho_v f_{yv}}{f_{c0}^{'}} \tag{3}$$

$$\varepsilon_{cu}=\varepsilon_{cc}+0.15/Z \tag{4}$$

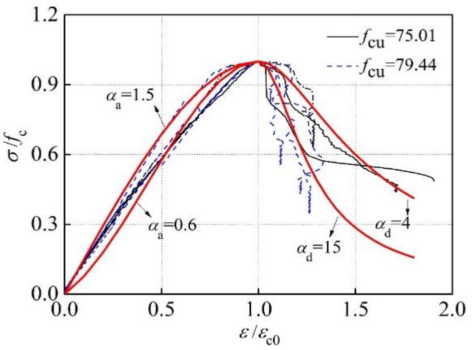

Fig. 9 Dimensionless stress-strain curve of HC

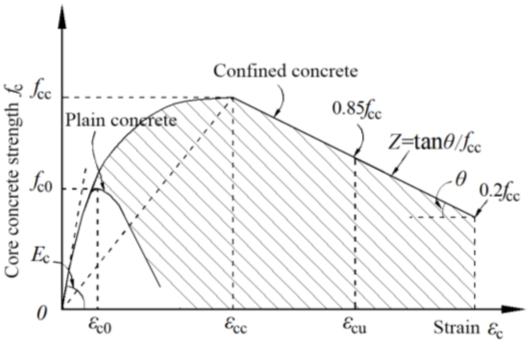

Fig. 10 Stress-strain curves for concrete core

And

$$Z=\frac{0.5}{\dfrac{3+0.29f_{c0}'}{145f_{c0}'-1000}+0.75\rho_v\sqrt{\dfrac{b'}{s}}-\varepsilon_{cc}} \tag{5}$$

Where ε_c is longitudinal strain in concrete, f_c is longitudinal stress in concrete (MPa), k is adjustment coefficient of considering stirrups confined, ε_{cc} is peak strain in concrete, ε_{c0}' is peak strain of plain concrete cylinder, ε_{cu} is ultimate compressive strain of confined concrete, used to the corresponding strain when the stress is reduced to 85% peak stress, Z is slope of descending section of curve, f_{cc} is peak stress in concrete, f_{c0}' is concrete compressive cylinder strength (MPa), approximate replacement of compressive strength f_{c0} of prismatic concrete, ρ_v is ratio of volume of hoop reinforcement to volume of concrete core measured to outside of the hoops, b' is width of concrete core measured to outside of the peripheral hoop (mm), s is center-to-center spacing of hoop sets (mm), f_{yv} is yield strength of hoop reinforcement.

The stress-strain curve of the high-strength concrete constitutive model consisted three parts: elastic stage, strength stage and softening stage, in which take the corresponding point of 1/3 peak stress (2013) as point ultimate elastic strain. The elastic modulus and Poisson's ratio were determined by experimental data or empirical formula respectively.

The plastic damage model was divided into plastic part and damage part. In this paper, only unidirectional push-over simulation was studied. To simplify the calculation, the damage part was not considered. The yield function F represents a space surface in the effective stress space, which determines the state of failure or damage of concrete member. Yield function expressed by effective stress

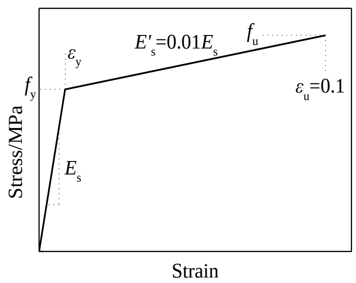

Fig. 11 Steel models for parametric study

$$F=\frac{1}{1-\alpha}\left[\sqrt{3J_2}+\alpha I_1+\beta\langle\sigma_{max}\rangle-\gamma\langle-\sigma_{max}\rangle\right]-\sigma_{c0} \tag{6}$$

$$\alpha=\frac{\sigma_{b0}/\sigma_{c0}-1}{2\sigma_{b0}/\sigma_{c0}-1}\quad \beta=\frac{\sigma_{c0}}{\sigma_{t0}}(1-\alpha)-(1+\alpha)\quad \gamma=\frac{3(1-K_c)}{2K_c-1} \tag{7}$$

Where I_1, J_2 are the first invariants of the stress tensor and second invariants of partial stress tensor, respectively, σ_{b0} is biaxial compressive strength of concrete, σ_{c0} is uniaxial compressive strength of concrete, the ratio of σ_{b0}/σ_{c0} suggests 1.16, σ_{t0} is uniaxial tensile strength of concrete, K_c is a parameter to control the projective shape of concrete yield surface on a deviated plane. For reinforced concrete, it was suggested that K_c=2/3.

The flow rule of concrete plastic model adopts the uncorrelated flow rule and the plastic potential energy G adopts Drucker-Prager hyperbolic function

$$G=\sqrt{(\lambda\sigma_{t0}\tan\psi)^2+1.5\rho^2}+\sqrt{3}\xi\tan\psi \tag{8}$$

Where $\rho=(2J_2)^{1/2}$ is Von-Mises equivalent stress, Ψ is expansion angle and the range of values is [37°, 42°], ξ is effective hydrostatic pressure, λ is offset parameter, representation the rate at which hyperbolic functions tend to asymptote, and value should be 0.1. Due to the non-correlation of the plastic flow of concrete, the unsymmetrical matrix method is used to calculation stiffness matrix of concrete.

4.1.2 Material model for the steel bar

The bi-linear stress-strain relationship for steel bar is illustrated in Fig. 11 and the calculation was given in Eq. 9. Young's modulus E_s was approximated as 200,000 MPa and the Young's modulus of steel after yield (Eq. 10); Poisson's ratio υ_s was set to be 0.3. Plastic behavior of the steel initiates at f_y, after which the stress increases up to f_u. The strain corresponding to f_u was approximated as 0.1, as shown in Fig. 11. To model the steel, the Von-Mises yield criterion and isotropic hardening model were applied. Stress-strain relationships for the verification models were constructed from the measured stress-strain curves obtained from material tests.

$$\begin{cases}\sigma=E_s\varepsilon & \varepsilon\le\varepsilon_y\\ \sigma=f_y+E_s'\varepsilon_s & \varepsilon>\varepsilon_y\end{cases} \tag{9}$$

$$E_s'=0.01E_s \tag{10}$$

Table 5 Comparison between experimental and predicted results

Specimens No.	Ultimate load		Ultimate displacement		Load	Displacement
	Analysis (kN)	Test (kN)	Analysis (mm)	Test (mm)	Analysis/Test	Analysis/Test
RHC-PVCT-1	194.70	196.54	7.05	11.47	0.99	0.61
RHC-PVCT-2	232.26	240.97	7.12	6.49	0.96	1.10
RHC-PVCT-3	186.17	179.65	11.26	14.97	1.04	0.75
RHC	179.06	182.00	7.95	9.96	0.98	0.80

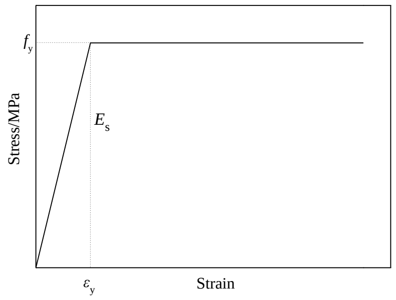

Fig. 12 PVCT models for parametric study

4.1.3 Material model for the PVCT

According to the measured stress-strain relationship curve of the material test of PVC tube, the ideal elastoplastic model is selected as the constitutive model of PVC material (Eq. (11)), as shown in Fig. 12. It is assumed that the PVCT follows the Von-Mises yield criterion and the related flow rule.

$$\begin{cases} \sigma = E_s\varepsilon & \varepsilon \le \varepsilon_y \\ \sigma = E_s\varepsilon_y = f_y & \varepsilon > \varepsilon_y \end{cases} \tag{11}$$

Where E_s is Young's modulus, f_y is yield strength.

4.2 FEM

In these models, 8-node reduced integral format 3D solid elements (C3D8R) were used to simulate the high-strength concrete and loading plate. As well, 4-node reduced integral format shell elements (S4R) were adopted for the PVCT. The steel bar adopted T3D2 element, that is, the 2-node three-dimensional truss element. To consider the calculation speed and accuracy, it was necessary to divide the mesh density reasonably. The size of the concrete element was determined to be 20 mm after several adjustments. The free mesh technique was used for both longitudinal bars and stirrups. Through the above measures were given sufficiently accurate results with quick convergence and reasonable computation time. The meshes at the contacting surfaces were matched to obtain the best accuracy in contact analysis. There was a change in cross-section size between the specimen and the foundation support.

As the study of bond-slip between PVCT and high-strength concrete is still blank, as a preliminary study, the definition of embed will be adopted in this paper.

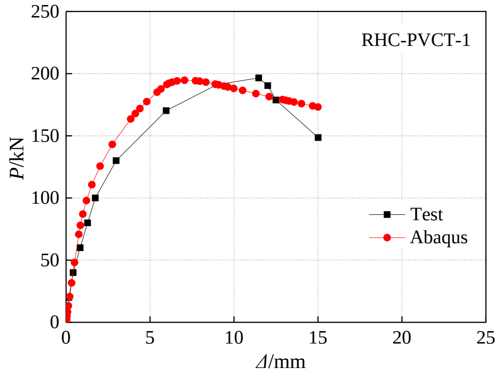

(a) RHC-PVCT-1 column

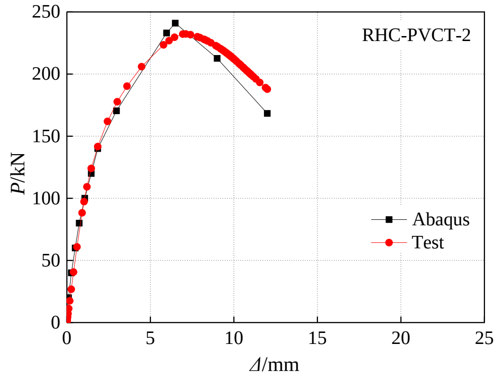

(b) RHC-PVCT-2 column

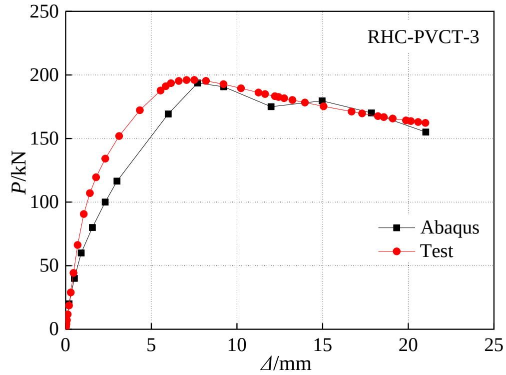

(c) RHC-PVCT-3 column

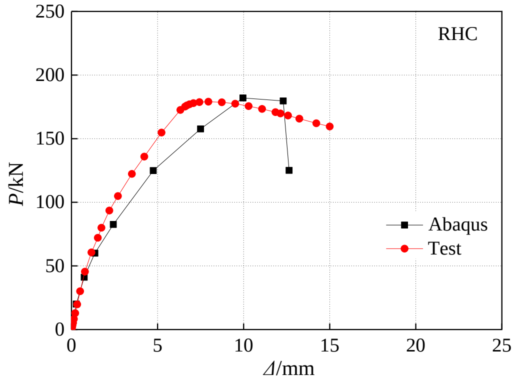

(d) RHC column

Fig. 13 Comparison between experimental and finite element simulation results for load-displacement curve

To make the boundary conditions and load applied mode of the FEM the same as the test condition, all section sizes

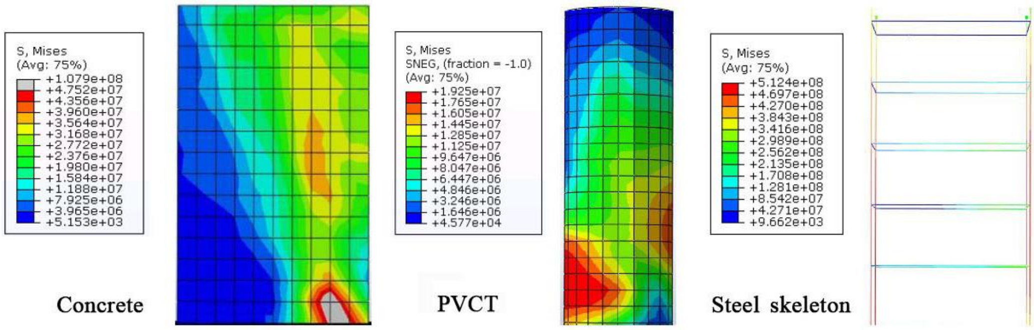

(a) RHC-PVCT-1 column

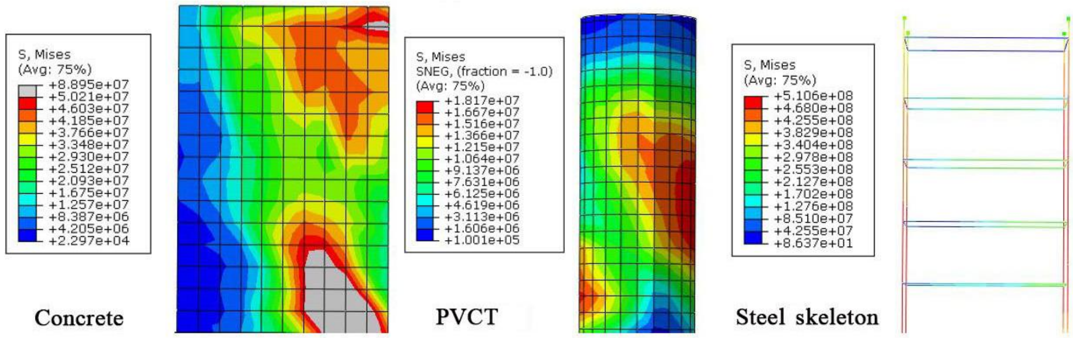

(b) RHC-PVCT-2 column

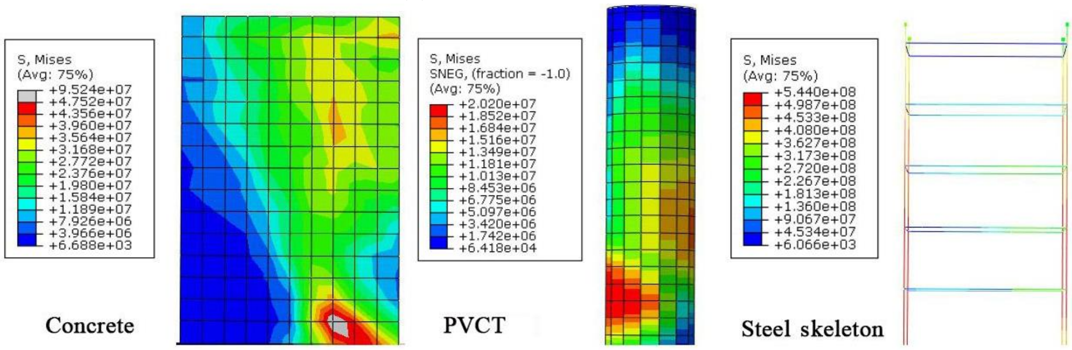

(c) RHC-PVCT-3 column

Fig. 14 Comparisons between various load-displacement relations of specimens

and reinforcement were determined according to the test model. The bottom of the FEM was fixed and the top was subjected to axial load and then horizontal load.

Three analytical steps were installed in the step module of the FEM. The initial step was set to fix the bottom of the model. The first step was applying the axial load to the design at the top of the model. The second step was applying horizontal load to the top of the model and the horizontal displacement was determined by the loading rules of the experiment.

4.3 Comparisons and discussion

The mechanical behavior of RHC-PVCT column under unidirectional load was simulated by ABAQUS. The calculated load-displacement skeleton curve is compared with the experimental results as shown in Fig. 13(a)-(d). The predicted values and the test values of ultimate loads and corresponding displacements of each column specimen are listed in Table 5.

From Figs. 13(a)-(d) and Table 5, the variation trend of the curve is basically similar and the deviation of the corresponding slightly displacement. There were three main reasons for this: firstly, the PVCT and the bond slip between steel bar and concrete were neglected in the model, which leads to the large stiffness of the FEM. Secondly, the unidirectional loading was applied in the ABAQUS calculation process. The values decreased of the stiffness calculation was more slowly than that in the experimental process due to the slight damage caused by the repeated loading. The third one was the error caused by the gap in the interface between the test equipment and the specimen.

Figs. 14(a)-(c) is the stress field diagram of the FEM of RHC-PVCT column. Compared with the Fig. 14 and Fig. 5, we can obtain that the failure patterns of RHC-PVCT columns in finite element simulation consistent with test phenomenon.

The simulation results from the skeleton curve, ultimate bearing capacity and failure form of the specimens were in good agreement with the experimental results. The FEM

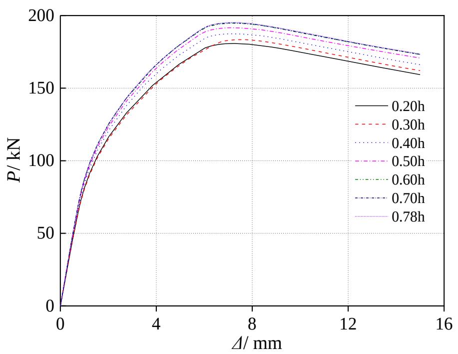

Fig. 15 Influence of the ratio of diameter to height

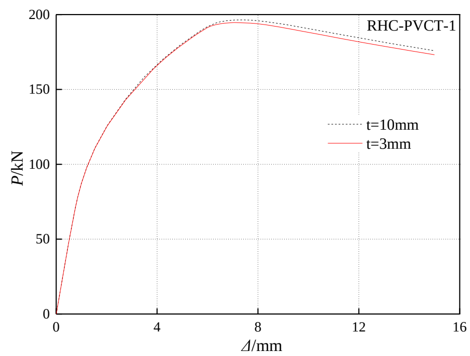

Fig. 16 Influence of the wall thickness

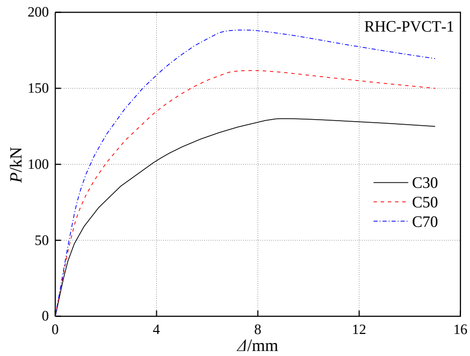

Fig. 17 Influence of the strength of concrete

established in this paper was used for the static elasto-plastic analysis of RHC-PVCT column.

5. Parametric study

A numerical modeling technique has been proposed based on above fiber element formulations for the determination of the performance of RHC-PVCT short columns made of each section subjected to seismic performance. The mathematical model proposed was utilized to examine the structural behavior of RHC-PVCT short columns. The mechanical properties of RHC-PVCT short column was affected by many factors. In this paper, the ratio of diameter to height of PVCT (*D*/*h*), the wall thickness of PVCT and the strength of concrete were analyzed.

5.1 Influences of the diameter to height ratio of PVCT

The effect of diameter to height ratio (*D*/*h*) of PVCT on the mechanical behavior of RHC-PVCT column was studied. Based on the experimental model for RHC-PVCT-1 column, the external diameter *D* of PVCT was changed meanwhile keeping the cross-section area of PVCT unchanged. PVCT having the diameter to height ratio of 0.20, 0.30, 0.40, 0.50, 0.60, 0.70 and 0.78 were used in the numerical analyses.

From Fig. 15, as the diameter-height ratio of PVCT rises, so does the initial stiffness and the ultimate loads of RHC-PVCT column, as well as the curves are parallel in failure stage which indicating the ductility unchanged. When the diameter to height ratio of PVCT is increased from 0.20 to 0.30, 0.40, 0.50, 0.60, 0.70 and 0.78, the peak loading of columns is found to increase by 1.4%, 3.7%, 6.0%, 7.7%, 7.9% and 8.0%, respectively, and the ultimate loading of columns is found to increase by 1.7%, 4.3%, 7.2%, 8.7%, 8.7% and 8.9%, respectively. Through the above analysis, the *D*/*h* value of PVCT in RHC-PVCT column about 0.5 had the best mechanical performance than other values.

5.2 Influences of the wall thickness of PVCT

Fig. 16 shows the ultimate load of the RHC-PVCT columns as a function of the wall thickness of PVCT when the core concrete strength is the same. As the wall thickness increases from 3 mm to 10 mm, the ultimate load of the RHC-PVCT-1 column is improved to some extent (Fig. 16). This is because after the ultimate bearing capacity of the RHC-PVCT-1 column, the core concrete breaks and the hoop strain increase sharply. The hoop stress from PVCT restricted the development of core concrete deformation. The thicker the PVCT wall, the larger the hoop constraint that can be provided, and the higher the peak loading of the RHC-PVCT column. When the wall thickness was changed from 3 mm to 10 mm, the ultimate load increased by 0.9%. The change of wall thickness had less effect on the ultimate load in the RHC-PVCT column.

5.3 Influences of the concrete strength

The influence of the concrete strength on the mechanical behavior of RHC-PVCT column was researched by changing the concrete strength of the FEM. The strength of concrete was taken at 30 MPa, 50 MPa and 70 MPa. Fig. 17 shows the influence of concrete strength on the load-displacement curve of RHC-PVCT columns. With the increase of concrete strength, the initial stiffness and peak load were greatly improved. When the concrete strength is increased from 30 MPa to 50 MPa and 70 MPa, the column ultimate strength is found to increase by 24.4% and 44.9%, respectively.

The result shows that the peak load of RHC-PVCT column is higher than that of ordinary reinforced high-strength concrete column and the peak load of RHC-PVCT columns is also increased by increasing the strength of HC. The failure load of models was reduced to 96.1% when 30

MPa of concrete strength, to 92.8% when 50 MPa of concrete strength and to 90.0% when 70 MPa of concrete strength, indicating that the strength reduction was accelerated with the increased of concrete strength.

6. Conclusions

The seismic behaviour of the 4 columns were tested in detail under lateral cyclic loading. Nonlinear FEM of ABAQUS models were employed to analyze the behavior of RHC-PVCT columns. The following conclusions can be made based on the test and analysis results:

- The all short columns occurred shear failure, and the RHC-PVCT short columns formed obvious X-shaped cross diagonal crack before failure and has good seismic performance.
- Compared with RHC column, hysteretic curves are fuller and the peak load and ultimate deformation are higher of RHC-PVCT column.
- FEM established by ABAQUS was used to simulate a new type of RHC-PVCT column. The simulated results of the load-displacement curve, ultimate loading and failure pattern were good agreement with the experimental results. The ABAQUS model established in this paper is reasonable and can be used for the elasto-plastic analysis of RHC-PVCT columns.
- For FEM of RHC-PVCT column, the influence of parameters such as wall thickness of PVCT, the ratio of diameter to height of PVCT and strength of concrete on the mechanical properties of column were studied. Increase in the diameter-height ratio of PVCT resulted in a corresponding increase in ultimate capacity and ductility. The PVCT can improve the energy dissipating and deformation capacity of RHC-PVCT column.

Acknowledgements

The research was funded by National Natural Science Foundation of China (No. 51608435), and Key Scientific and Technological Innovation Team of Shaanxi Province (No. 2019TD-029), which is gratefully acknowledged.

References

Benzaid, R., Mesbah, H. and Chikh, N.E. (2010), “FRP-confined concrete cylinders: axial compression experiments and strength model”, *J. Reinf. Plast. Compos.*, **29**(16), 2469-2488.

Bisby, L.A., Dent, A.J. and Green, M.F. (2005), “Comparison of confinement models for fiber reinforced polymer-wrapped concrete”, *ACI Struct. J.*, **102**(1), 62-72.

Boersma, A. and Breen, J. (2005), “Long term performance prediction of existing PVC water distribution systems”, *9th International Conference PVC*, Brighton, England.

Borges, D.C. and Pituba, J.J. (2017), “Analysis of quasi-brittle materials at mesoscopic level using homogenization model”, *Adv. Concr. Constr.*, **5**(3), 221-240.

Breen, J. (2006), “Expected lifetime of existing water distribution systems-management summary”, TNO Report MT-RAP-06-18692/MSO, TNO Science and Industry.

Burn, S., Davis, P. and Schiller, T. (2006), “Long-term performance prediction for PVC pipes”, American Water Works Association AWWARF, Report 91092F.

Chen, Y., Feng, R. and Xiong, L. (2016), “Experimental and numerical investigations on steel-concrete-PVC SHS joints under axial compression”, *Constr. Build. Mater.*, **102**, 654-670.

CMC (2002), GB/T228-2002, Metallic Materials-Tensile Testing-Method of Test at Ambient Temperature, China Ministry of Construction; Beijing, China.

CMC (2003), GB/T 8804.1-2003, Thermoplastic Pipes-Determination of Tensile Properties-Part 1: General Test Method, China Ministry of Construction; Beijing, China.

CMC (2015), JGJ 101-2015, Specification for seismic test of buildings, China Ministry of Construction; Beijing, China.

Fakharifar, M. and Chen, M.G. (2016), “Compressive behavior of FRP-confined concrete filled PVC tubular columns”, *Compos. Struct.*, **141**, 91-109.

Fakharifar, M. and Chen, M.G. (2017), “FRP-confined concrete filled PVC tubes: a new design concept for ductile column construction n in seismic regions”, *Constr. Build. Mater.*, **130**, 1-10.

Folkman, S. (2014), “Validation of the long life of PVC pipes”, *Proceedings of the 17thPlastic Pipes Conference PPXVII*, Chicago, Illinois, USA.

Hosseinpour, F. and Abdelnaby, A.E. (2015), “Statistical evaluation of the monotonic models for FRP confined concrete prisms”, *Adv. Concrete Constr.*, **3**(3), 161-185.

Jiang, S., Ma, S. and Wu, Z. (2014), “Experimental study and theoretical analysis on slender concrete-filled CFRP–PVC tubular columns”, *Constr. Build. Mater.*, **53**(2), 475-487.

Kumar, C.N.S., Krishna, P. and Kumar, D.R. (2017), “Effect of fiber and aggregate size on mode-I fracture parameters of high strength concrete”, *Adv. Concrete Constr.*, **5**(6), 613-624.

Kurt, E.C. (1978), “Concrete filled structural plastic columns”, *Proceedings ASCE104 ST1*, 55-63.

Lam, L. and Teng, J. (2003), “Design-oriented stress–strain model for FRP-confined concrete”, *Constr. Build. Mater.*, **17**(6), 471-489.

Ma, C.K., Awang, A.Z. and Omar, W. (2016), “Flexural ductility design of confined high-strength concrete columns: theoretical modelling”, *Measure.*, **78**, 42-48.

Ma, C.K., Awang, A.Z., Omar, W. and Maybelle, L. (2014), “Experimental tests on SSTT-confined HSC columns”, *Mag. Concrete Res.*, **66**(21), 1084-1094.

Mesbah, H.A. and Benzaid, R. (2017), “Damage-based stress-strain model of RC cylinders wrapped with CFRP composites”, *Adv. Concrete Constr.*, **5**(5), 539-561.

Murthy, A.R., Iyer, N.R. and Prasad, B.K. (2013), “Evaluation of mechanical properties for high strength and ultrahigh strength concretes”, *Adv. Concrete Constr.*, **1**(4), 341-358.

Nie, J.G. and Wang, Y.H. (2013), “Comparison study of constitutive model of concrete in Abaqus for static analysis of structures”, *Eng. Mech.*, **30**(4), 59-67. (in Chinese)

Ognedal, A.S., Clausen, A.H., Dahlen, A. and Hopperstad, O.S. (2014), “Behavior of PVC and HDPE under highly triaxial stress states: an experimental and numerical study”, *Mech. Mater.*, **72**(5), 94-108.

Ognedal, A.S., Clausen, A.H., Polanco-Loria, M., Benallal, A., Raka, B. and Hopperstad, O.S. (2012), “Experimental and numerical study on the behaviour of PVC and HDPE in biaxial tension”, *Mech. Mater.*, **54**, 18-31.

Ozbakkaloglu, T. and Lim, J.C. (2013), “Axial compressive behavior of FRP-confined concrete: experimental test database and a new design-oriented model”, *Compos. Part B Eng.*, **55**, 607-634.

Ozbakkaloglu, T., Lim, J.C. and Vincent, T. (2013), “FRP-confined concrete in circular sections: review and assessment of stress-strain models", *Eng. Struct.*, **49**, 1068-1088.

Saafi, M. (2005), "Development and Behavior of a New Hybrid Column in Infrastructure Systems", Ph.D. Dissertation; University of Alabama in Huntsville, Alabama, USA.

Scott, B.D., Park, R. and Prisetley, M.J.N. (1982), "Stress-Strain behavior of concrete confined by overlapping hoops at low and high strain rates", *ACI J.*, **79**(2), 13-27.

Shehata, I.A.E.M., Carneiro, L.A.V. and Shehata, L.C.D. (2002), "Strength of short concrete columns confined with CFRP sheets", *Mater. Struct.*, **35**(1), 50-58.

Toutanji, H. (2001), "Design equations for concrete columns confined with hybrid composite materials", Adv. *Compos. Mater.*, **10**(2-3), 127-138.

Toutanji, H. and Saafi, M. (2001), "Durability studies on concrete columns encased in PVC-FRP composite tubes", *Compos. Struct.*, **54** (1), 27-35.

Toutanji, H. and Saafi, M. (2002), "Stress-strain behavior of concrete columns confined with hybrid composite materials", *Mater. Struct.*, **35**(6), 338-347.

Wang, J.Y. and Yang, Q.B. (2012), "Investigation on compressive behaviors of thermoplastic pipe confined concrete", *Constr. Build. Mater.*, **35** (35), 578-585.

Wei, Y.Y. and Wu, Y.F. (2012), "Unified stress-strain model of concrete for FRP-confined columns", *Constr. Build. Mater.*, **26**(1), 381-392.

Youssef, M.N., Feng, M.Q. and, Mosallam, A.S. (2007), "Stress–strain model for concrete confined by FRP composites", *Compos. Part B Eng.*, **38**(5), 614-628.

CC